J|A|C|S
ARTICLES

Published on Web 10/07/2009

Understanding Ground- and Excited-State Properties of Perylene Tetracarboxylic Acid Bisimide Crystals by Means of Quantum Chemical Computations

Hong-Mei Zhao,[†] Johannes Pfister,[†] Volker Settels,[†] Manuel Renz,[‡] Martin Kaupp,*[,‡] Volker C. Dehm,[†] Frank Würthner,[†] Reinhold F. Fink,*[,†] and Bernd Engels*[,†]

Institute of Organic Chemistry, and Institute of Inorganic Chemistry, University of Würzburg, Am Hubland, D-97074 Würzburg, Germany

Received March 30, 2009; E-mail: bernd@chemie.uni-wuerzburg.de; reinhold.fink@uni-wuerzburg.de; kaupp@mail.uni-wuerzburg.de

Abstract: Quantum chemical protocols explaining the crystal structures and the visible light absorption properties of 3,4:9,10-perylene tetracarboxylic acid bisimide (PBI) derivates are proposed. Dispersion-corrected density functional theory has provided an intermolecular potential energy of PBI dimers showing several energetically low-lying minima, which corresponds well with the packing of different PBI dyes in the solid state. While the dispersion interaction is found to be crucial for the binding strength, the minimum structures of the PESs are best explained by electrostatic interactions. Furthermore, a method is introduced, which reproduces the photon energies at the absorption maxima of PBI pigments within 0.1 eV. It is based on time-dependent Hartree−Fock (TD-HF) excitation energies calculated for PBI dimers with the next-neighbor arrangement in the pigment and incorporates crystal packing effects. This success provides clear evidence that the electronically excited states, which determine the color of these pigments, have no significant charge-transfer character. The developed protocols can be applied in a routine manner to understand and to predict the properties of such pigments, which are important materials for organic solar cells and (opto-)electronic devices.

1. Introduction

Functional π-conjugated molecules with charge and energy transport properties are intensively investigated in biological as well as in material science.[1] In the latter area, the class of perylene tetracarboxylic acid bisimides, also named perylene bisimides (PBIs), possess very favorable properties such as light resistance,[2] intense photoluminescence,[3] and outstanding n-type semiconductive properties,[4] making them particularly interesting for applications in organic solar cells,[5] organic transistors,[6] organic light emitting diodes,[7] and other (opto-)electronic devices.[8] Additionally, PBI derivatives have been used for

[†] Institute of Organic Chemistry.
[‡] Institute of Inorganic Chemistry.

(1) (a) Pullerits, T.; Sundström, V. *Acc. Chem. Res.* **1996**, *29*, 381–389. (b) Grimsdale, A. C.; Müllen, K. *Angew. Chem., Int. Ed.* **2005**, *44*, 5592–5629. (c) Poulsen, L.; Jazdzyk, M.; Communal, J.-E.; Sancho-Garcia, J. C.; Mura, A.; Bongiovanni, G.; Beljonne, D.; Cornil, J.; Hanack, M.; Egelhaaf, H.-J.; Gierschner, J. *J. Am. Chem. Soc.* **2007**, *129*, 8585–8593. (d) Sancho-García, J. C.; Pérez-Jiménez, A. J. *J. Chem. Phys.* **2008**, *129*, 024103. (e) Damjanovic, A.; Kosztin, I.; Kleinekathöfer, U.; Schulten, K. *Phys. Rev. E* **2002**, *65*, 031919.

(2) Herbst, W.; Hunger, K. *Industrial Organic Pigments: Production, Properties, Applications*, 2nd ed.; Wiley−VCH: Weinheim, 1997.

(3) Langhals, H.; Karolin, J.; Johansson, L. B. *J. Chem. Soc., Faraday Trans.* **1998**, *94*, 2919–2922.

(4) (a) Struijk, C. W.; Sieval, A. B.; Dakhorst, J. E. J.; van Dijk, M.; Kimkes, P.; Koehorst, R. B. M.; Donker, H.; Schaafsma, T. J.; Picken, S. J.; van de Craats, A. M.; Warman, J. M.; Zuilhof, H.; Sudholter, E. J. R. *J. Am. Chem. Soc.* **2000**, *122*, 11057–11066. (b) Dimitrakopoulos, C. D.; Malenfant, P. R. L. *Adv. Mater.* **2002**, *14*, 99–117. (c) Lee, S. K.; Zu, Y.; Herrmann, A.; Geerts, Y.; Müllen, K.; Bard, A. J. *J. Am. Chem. Soc.* **1999**, *121*, 3513–3520. (d) Horowitz, G.; Kouki, F.; Spearman, P.; Fichou, D.; Nogues, C.; Pan, X.; Garnier, F. *Adv. Mater.* **1996**, *8*, 242–245.

(5) (a) Tang, C. W. *Appl. Phys. Lett.* **1986**, *48*, 183–185. (b) Schmidt-Mende, L.; Fechtenkötter, A.; Müllen, K.; Moons, E.; Friend, R. H.; MacKenzie, J. D. *Appl. Sci.* **2001**, *293*, 1119–1122. (c) Peumans, P.; Uchida, S.; Forrest, S. R. *Nature* **2003**, *425*, 158–161.

(6) (a) Jones, B. A.; Facchetti, A.; Wasielewski, M. R.; Marks, T. J. *J. Am. Chem. Soc.* **2007**, *129*, 15259–15278. (b) Jones, B. A.; Facchetti, A.; Wasielewski, M. R.; Marks, T. J. *Adv. Funct. Mater.* **2008**, *18*, 1329–1339. (c) Weitz, R. T.; Amsharov, K.; Zschieschang, U.; Villas, E. B.; Goswami, D. K.; Burghard, M.; Dosch, H.; Jansen, M.; Kern, K.; Klauk, H. *J. Am. Chem. Soc.* **2008**, *130*, 4637–4645. (d) Schmidt, R.; Ling, M.-M.; Oh, J. H.; Winkler, M.; Könemann, M.; Bao, Z.; Würthner, F. *Adv. Mater.* **2007**, *19*, 3692–3695. (e) Oh, J. H.; Liu, S.; Bao, Z.; Schmidt, R.; Würthner, F. *Appl. Phys. Lett.* **2007**, *91*, 212107.

(7) (a) Ranke, P.; Bleyl, I.; Simmer, J.; Haarer, D.; Bacher, A.; Schmidt, H. W. *Appl. Phys. Lett.* **1997**, *71*, 1332–1334. (b) Pandey, A. K.; Nunzi, J.-M. *Appl. Phys. Lett.* **2007**, *90*, 263508(1−3). (c) Jaiser, F.; Neher, D.; Meisel, A.; Nothofer, H.-G.; Miteva, T.; Herrmann, A.; Müllen, K.; Scherf, U. *J. Chem. Phys.* **2008**, *129*, 114901(1−9). (d) Ego, C.; Marsitzky, D.; Becker, S.; Zhang, J.; Grimsdale, A. C.; Müllen, K.; MacKenzie, J. D.; Silva, C.; Friend, R. H. *J. Am. Chem. Soc.* **2003**, *125*, 437–443.

(8) (a) Langhals, H. *Heterocycles* **1995**, *40*, 477–500. (b) Würthner, F. *Chem. Commun.* **2004**, 1564–1579. (c) Law, K.-Y. *Chem. Rev.* **1993**, *93*, 449–486. (d) Gregg, B. A. *J. Phys. Chem.* **1996**, *100*, 852–859. (e) Mizuguchi, J. *J. Appl. Phys.* **1998**, *84*, 4479–4486. (f) Mizuguchi, J.; Hino, K.; Tojo, K. *Dyes Pigm.* **2006**, *70*, 126–135. (g) Mizuguchi, J. *Dyes Pigm.* **2006**, *70*, 226–231. (h) Chen, Z.; Lohr, A.; Saha-Möller, C. R.; Würthner, F. *Chem. Soc. Rev.* **2009**, *38*, 564–584.

 10.1021/ja902512e CCC: $40.75

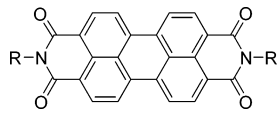

Figure 1. The planar perylene tetracarboxylic bisimide (PBI) moiety that is common to all derivatives investigated by Klebe et al.[9]

decades as organic high-performance pigments with color shades from red, via maroon, to black.[2,9,11]

Optical as well as charge and energy transport properties of functional π-conjugated molecules strongly depend on intermolecular interactions and on the mutual orientation of the monomers.[10] Hence, a rational design of functionalities requires a detailed knowledge on how the geometrical orientation of the molecules within the solid state or in thin films influences these properties. Klebe et al. investigated such relationships for the example of 18 differently substituted perylene bisimides, which exhibit different substituents at the imide nitrogen atoms (Figure 1).[9] Because some of them form more than one polymorph, the data set covers 24 different structures for which geometrical arrangements and absorption maxima are available. In the crystal, most of them are arranged in stacks with parallel orientations of the flat perylene cores with longitudinal and transversal offsets between neighboring PBIs. The absorption maxima of the crystalline PBI pigments range from around 500 to about 680 nm. The importance of crystal packing for the color is underlined by the fact that the absorption maxima of dilute solutions or molecular dispersions of PBIs, in which short-range interactions can be excluded, vary merely between 520 and 530 nm. Twenty-one structures of the solid-state data set exhibit absorption maxima, which are red-shifted with respect to the absorption spectra of the monomer. Only three structures exhibit a blue shift. Klebe et al.[9,11] presented an empirical fit, which correlates the absorption maxima (λ_{max}) of the pigments with the longitudinal (X) and transversal (Y) offsets between next-neighbor PBIs.

$$\lambda_{max} = 9.718(\pm 3.03)Y^2 - 82.009(\pm 20.74)Y - 21.888(\pm 9.30)X + 735.329$$

Trends could be nicely reproduced by the formula. However, it does not explain the influence of transversal and longitudinal shifts on the absorption wavelength, and it does not provide a picture of the nature of the excited states. Such insights, however, are important for a further design of extended π-conjugated molecules with desired properties. Hence, tight-binding extended Hückel calculations were used to simulate the trends in the wavelength maximum and the broadening of the absorption as a function of the one-dimensional geometry.[12] Other investigations focused on the crystal geometries, which were investigated using different force fields and optimization routines.[13,14] A molecular dynamics simulation of possible crystal structures of the PBI derivative with R = CH_3 was recently performed by Zykova-Timan et al.[15] They were able to predict the correct crystal structure and additional polymorphs but concentrated on this single derivative. Several semiempirical quantum chemical calculations were performed to study the influence of the mutual orientation on the absorption spectra.[16,17]

Despite these efforts, many questions are still open. The strong variations in the crystal structures indicate clearly that the substitution pattern influences the three-dimensional packing of these dyes considerably. However, the importance of the interactions between the large π-systems of the PBI cores for the crystal structure is unclear. The character of the involved low-lying electronically excited states is also still under debate. For 3,4:9,10-perylene tetracarboxylic dianhydride (PTCDA), Forrest and co-workers identified an extended free charge-transfer (CT) state at about 2.2 eV.[18] Comparable features were also discussed by Gregg and co-workers,[19] Gomez et al.,[20] and Scholz et al.[21] A theoretical approach of Hoffmann et al.[22] supported the importance of CT states for the PTCDA absorption spectrum. They used an empirical Hamiltonian based on a one-dimensional stack model to simulate the PTCDA absorption spectrum. This Hamiltonian contained a strong exciton−phonon coupling but included a simplified ansatz for vibronic effects. The authors conclude that CT states have a strong influence on the absorption spectrum because agreement between theory and experiment is only found if excitations to charge-transfer states are included in the empirical Hamiltonian. Their results also indicate a strong mixing between CT and neutral states. The work was extended to thin films of MePTCDI crystals (Figure 1 with R = CH_3). Here again, the results indicate the involvement of CT states. It is important to note that the employed model Hamiltonians do not include motions of the monomers with respect to each other. Charge-transfer states also seem to play a central role in the dissociation of excitons.[23]

However, recent experimental investigations do not support the involvement of charge-transfer states in the fluorescence spectra of π-stacked H-aggregates.[24] Theoretical investigations that support the importance of CT states on the basis of time-dependent density functional theory (TD-DFT) computations[25] are questionable[26] because the energy of CT states is heavily underestimated by this approach.[27] Recent investigations showed that this failure of standard TD-DFT does not only influence

(9) Klebe, G.; Graser, F.; Hädicke, E.; Berndt, J. *Acta Crystallogr.* **1989**, *B45*, 69–77.
(10) (a) Cornil, J.; Beljonne, D.; Calbert, J.-P.; Brédas, J.-L. *Adv. Mater.* **2001**, *13*, 1053–1067. (b) Hippius, C.; van Stokkum, I. H. M.; Zangrando, E.; Williams, R. M.; Wykes, M.; Beljonne, D.; Würthner, F. *J. Phys. Chem. C* **2008**, *112*, 14626–14638. (c) Burquel, A.; Lemaur, V.; Beljonne, D.; Lazzaroni, R.; Cornil, J. *J. Phys. Chem. A* **2006**, *110*, 3447–3453.
(11) Graser, F.; Hädicke, E. *Liebigs Ann. Chem.* **1984**, 483–494.
(12) Kazmaier, P. M.; Hoffmann, R. *J. Am. Chem. Soc.* **1994**, *116*, 9684–9691.
(13) Perlstein, J. *Chem. Mater.* **1994**, *6*, 319–326.
(14) McKerrow, A. J.; Buncel, E.; Kazmaier, P. M. *Can. J. Chem.* **1993**, *71*, 390–398.
(15) Zykova-Timan, T.; Raiteri, P.; Parrinello, M. *J. Phys. Chem. B* **2008**, *112*, 13231–13237.
(16) (a) Mizuguchi, J.; Tojo, K. *J. Phys. Chem. B* **2002**, *106*, 767–772. (b) Donati, F.; Pucci, A.; Cappelli, C.; Mennucci, B.; Ruggeri, G. *J. Phys. Chem. B* **2008**, *112*, 3668–3679.
(17) Marcon, V.; Kirkpatrick, J.; Pisula, W.; Andrienko, D. *Phys. Status Solidi B* **2008**, *245*, 820–824.
(18) Bulovic, V.; Burrows, P. E.; Forrest, S. R.; Cronin, J. A.; Thompson, M. E. *Chem. Phys.* **1996**, *210*, 1–12.
(19) (a) Gregg, B. A. *J. Phys. Chem. B* **2003**, *107*, 4688–4698. (b) Gregg, B. A.; Hanna, M. C. *J. Appl. Phys.* **2003**, *93*, 3605–3614. (c) Gregg, B. A. *J. Phys. Chem.* **1996**, *100*, 852–859. (d) Conboy, J. C.; Olson, E. J. C.; Adams, D. M.; Kerimo, J.; Zabau, A.; Gregg, B. A.; Barbara, P. F. *J. Phys. Chem. B* **1998**, *102*, 4516–4525.
(20) Gomez, U.; Leonhardt, M.; Port, H.; Wolf, H. C. *Chem. Phys. Lett.* **1997**, *268*, 1–6.
(21) Scholz, R.; Kobitski, A. Y.; Zahn, D. R. T.; Schreiber, M. *Phys. Rev. B* **2005**, *72*, 245208.
(22) M Hoffmann, M.; Schmidt, K.; Fritz, T.; Hasche, T.; Agranovich, V. M.; Leo, K. *Chem. Phys.* **2000**, *258*, 73–96; **2000**, *258*, 73−96.
(23) Scholes, G. D. *ACS Nano* **2008**, *2*, 523–537.
(24) Giaimo, J. M.; Lockard, J. V.; Sinks, L. E.; Scott, A. M.; Wilson, T. M.; Wasielewski, M. R. *J. Phys. Chem. A* **2008**, *112*, 2322–2330.
(25) Clark, A. E.; Qin, C.; Li, A. D. Q. *J. Am. Chem. Soc.* **2007**, *129*, 7586–7595.

the predicted position of the CT states but also the computed shape of the potential energy surfaces of close-lying neutral states. The errors are due to the wrong energy order of CT and neutral states. This causes the interactions between both types of states to be predicted incorrectly. Deficiencies of TD-DFT methods for such aggregate structures are also shown in a recent study on the CD spectra of the merocyanine dimer.[28]

A recent theoretical study that could profoundly explain absorption and emission spectra of PBI aggregates in methylcyclohexane[29] gave also no indication for the involvement of charge-transfer states.[30] The assignment of absorption and emission spectra was based on potential-energy surfaces of the lowest-lying excited 1^1B_2 and the 1^1B_1 states. They result from the plus and minus linear combinations of the locally excited states and possess neutral characters. In that study, the RI-BLYP-D approach[31] was employed to obtain the ground-state surface, while a scaled TD-HF method[30] was used to compute excitation energies. This model predicts that photoabsorption leads preferentially to the higher 1^1B_1 state. However, its population is rapidly transferred to the lower-lying 1^1B_2 state via a conical intersection. The strongly red-shifted fluorescence of the PBI aggregates results from different geometrical arrangements of the dimers in the ground-state X^1A_1 (30° twisted structure) and in the excited 1^1B_2 state (eclipsed structure). This assignment points to a self-trapping mechanism without the involvement of charge-transfer states. While the agreement between this theoretical approach and the experimental data is very convincing, it remains to be seen whether this explanation holds also for other dimer structures, and if it can be extended to the solid state.

These questions are investigated in the present work. In a first step, the ground-state energy surface of an unsubstituted PBI dimer is computed, and the resulting minima are correlated with the crystal structures of the 18 differently substituted PBI derivatives investigated by Klebe et al.[9] We focus on this data set, as a similarly consistent and accurate set of absorption maxima and crystal structures is not available for other PBI derivatives. This analysis provides insight into the interplay of the interactions, which determine the crystal structure of PBI compounds. In the second step, the vertical excitation energies of 18 crystal structures are computed and correlated with the measured absorption maxima (λ_{max}) of the pigments. The results clearly pinpoint the nature of the states (neutral rather than CT), which determine the color and related optical properties of crystalline PBI pigments.

2. Computational Details

The ground-state potential energy surface (PES) for the PBI dimer was computed with the dispersion-corrected DFT-D method[31] using the BLYP functional[32,33] in combination with the dispersion parameters published by Grimme in 2004. The BLYP variant of the DFT-D method was chosen, because it represents an extensively validated approach yielding reliable interaction energies and structures for a wide variety of aggregate systems, in particular those with significant $\pi-\pi$ interactions.[34] The semiempirical dispersion correction of this method turned out to be absolutely essential. For the original BLYP method that does not include dispersion correction terms, monomer−monomer distances of more than 6.1 Å are obtained, and binding energies of less than 1 kcal mol^{-1} are predicted (no binding left after BSSE correction).

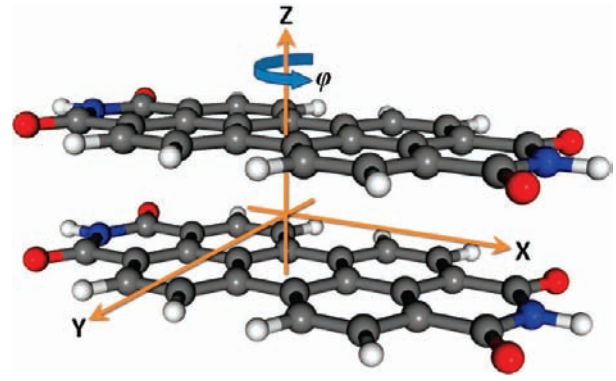

Figure 2. Intermolecular coordinates used for scanning the dimer potential energy surface (PES).

In all computations, the resolution-of-the-identity (RI) approximation was employed.[35] The TZVP[36] basis for C, N, and O was combined with a TZV[38] basis for H, and the TZVP auxiliary basis sets were employed to represent the charge density in the RI approach.[37] This basis, designated as TZV(P) in the following, was found to be an excellent compromise between accuracy and computational effort.[30] Binding energies predicted by this approach agree very well with higher-level benchmark computations (counterpoise-corrected SCS-MP2/QZVPP).[30] In the following, the combination of the BLYP-D variant of the DFT-D method with the TZV(P) basis is designated as RI-BLYP-D. All computations were performed with the TURBOMOLE program package (versions 5.9 and 5.9.1).[38]

After an initial search for low-lying minima with force-field methods, a PES scan (RI-BLYP-D) was carried out along the intermolecular coordinates shown in Figure 2. The geometrical structures of the monomers, which had been obtained with the same approach, were kept fixed during the scan. The distance between the monomer planes, R, was set to 3.4 Å, which is typically found experimentally. This is also close to the value obtained for the global minimum.[30] For the scan, the longitudinal (X) and transversal (Y) displacements of one monomer (Figure 2) were varied for $\varphi = 0°$, 30°, 60°, and 90°. Data points were computed every 0.25 Å from 0 to 4 Å for longitudinal displacement X and from 0 to 3 Å for transversal displacement Y (step size = 0.5 Å when $Y > 2.5$ Å). Exploiting the symmetry of the dimer system, the PESs within the ranges -4 Å $\leq X \leq 4$ Å and -3.0 Å $\leq Y \leq 3.0$ Å are obtained. For $\varphi = 0°$, the grid ranges are 0 Å $\leq X \leq 11.5$ Å and 0 Å $\leq Y \leq 4$ Å with intervals of 0.25 Å (stepsize = 0.5 Å for $Y > 2.5$ Å). Also for $\varphi = 0°$, the symmetry of the system was used to reduce the number of explicit computations.

(26) Fink, R. F.; Pfister, J.; Schneider, A.; Zhao, H.; Engels, B. *Chem. Phys.* **2008**, *343*, 353–362. Fink, R. F.; Pfister, J.; Zhao, H.; Engels, B. *Chem. Phys.* **2008**, *346*, 275–285.
(27) Dreuw, A.; Head-Gordon, M. *J. Am. Chem. Soc.* **2004**, *126*, 4007–4016.
(28) Goerigk, L.; Grimme, S. *ChemPhysChem* **2008**, *9*, 2467–2470.
(29) Seibt, J.; Marquetand, P.; Engel, V.; Chen, Z.; Dehm, V.; Würthner, F. *Chem. Phys.* **2006**, *328*, 354–361.
(30) Fink, R. F.; Seibt, J.; Engel, V.; Renz, M.; Kaupp, M.; Lochbrunner, S.; Zhao, H.; Pfister, J.; Würthner, F.; Engels, B. *J. Am. Chem. Soc.* **2008**, *130*, 12858–12859.
(31) Grimme, S. *J. Comput. Chem.* **2004**, *25*, 1463–1473.
(32) Becke, A. D. *Phys. Rev. A* **1988**, *38*, 3098–3100.
(33) Lee, C.; Yang, W.; Parr, R. G. *Phys. Rev. B: Condens. Matter* **1988**, *37*, 785–789.
(34) See, for example: Piacenza, M.; Grimme, S. *ChemPhysChem* **2005**, *6*, 1554. Antony, J.; Grimme, S. *Phys. Chem. Chem. Phys.* **2006**, *8*, 5287. Grimme, S.; Antony, J.; Schwabe, T.; Mück-Lichtenfeld, C. *Org. Biomol. Chem.* **2007**, *5*, 741.
(35) Treutler, O.; Ahlrichs, R. *J. Chem. Phys.* **1995**, *102*, 346–354.
(36) Schäfer, A.; Huber, C.; Ahlrichs, R. *J. Chem. Phys.* **1994**, *100*, 5829–5835.
(37) Eichkorn, K.; Weigend, F.; Treutler, O.; Ahlrichs, R. *Theor. Chim. Acta* **1997**, *97*, 119–124.
(38) Ahlrichs, R. *TURBOMOLE (since 1988), Version 5.9*; University of Karlsruhe: Germany, 2008.

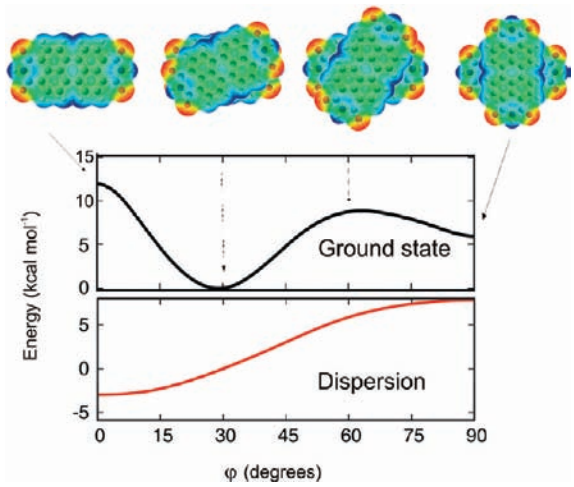

Figure 3. RI-BLYP-D potential energy curve of the electronic ground states and the dispersion contribution to the total energy as a function of the torsion angle φ. All values are given with respect to the global minimum (φ = 29.4°). Transversal and longitudinal displacements are zero ($X = Y = 0$ Å), and the distance between the two PBI cores is 3.4 Å. In the top panel, electrostatic potential surfaces of the PBI dimers are shown. Positively and negatively charged regions are indicated in blue and red, respectively.

The geometrical arrangements of the minima found in these scans were fully optimized without any constraint. In some cases, two different minima of the scan moved to the same minimum during the minimization. To analyze the minima, electrostatic potential surfaces were computed and represented with the GaussView 3.0 program.[39] TD-HF[40] was employed to compute vertical excitation energies. These computations were also performed with the TZV(P) basis set. To evaluate the performance of TD-DFT approaches, vertical excitation energies were additionally computed at the B3LYP/TZV(P) level of theory.

3. Results and Discussion

Ground-State Potential Energy Surface and Its Correlation with X-ray Structure Data. In our previous study,[29] the global minimum of the ground-state energy surface of the PBI dimer was found for a twisted arrangement of the monomers with $\varphi \approx 30°$. Figure 3 displays the shape of the ground-state potential as a function of φ ($X = Y = 0$ Å) together with the dispersion contribution obtained with the (BLYP) DFT-D approach and a pictorial representation of the electrostatic interactions. The energies are given with respect to the global minimum (vide infra). The figure shows that the eclipsed structure ($\varphi = 0°$) represents a maximum because the electrostatic interactions between the functional groups, which stand on top of each other, are repulsive (Figure 3, leftmost upper panel). This repulsion may also be explained as the interaction of the quadrupole moments of the PBI molecules. The quadrupole moment of the PBI monomer amounts to about −37 au and consists almost completely of the Θ_{XX}-component. It should be mentioned, however, that the actual electrostatic interaction energy of the PBI molecules in the eclipsed structure at a distance $R = 3.40$ Å is not well described by the quadrupole−quadrupole interaction, which amounts to roughly +180 kcal mol^{-1}. For further details about the quadrupole moments, see the Supporting Information.

Table 1. Stationary Points of the Ground-State PES Relevant for Known Crystal Structures[a]

	ΔE	[b]ΔE_{zero}	[c]ΔE_{disp}	R	X	Y	φ
SP1	0.0	0.0	0.0	3.36	0.00	0.00	29.4
SP2	4.3	1.1	2.4	3.36	0.92	1.40	0.0
SP3	5.9	1.3	2.1	3.40	1.54	0.00	0.0
SP4	4.5	−0.4	7.9	3.37	3.39	1.14	0.0
SP5	7.2	1.5	6.3	3.39	2.95	0.10	0.0
SP6	9.0	1.0	15.2	3.31	5.23	1.43	0.0
SP7	7.9	−1.0	15.9	3.45	5.58	0.00	0.0

[a] The energies are given relative to the global minimum SP1, including zero-point vibrational energies (RI-BLYP-D/TZV(P) level). Energies are given in kcal mol^{-1}, and distances and angles are in angstroms and degree, respectively. [b] Zero-point vibrational energy relative to SP1. [c] Contribution of the dispersion energy relative to SP1.

For $\varphi \approx 30°$, the partially negatively charged carbonyl oxygen atoms and the partially positively charged imide nitrogen atoms are close to each other. As a consequence, the attractive electrostatic interactions overcompensate the slight decrease of the attractive dispersion contribution, which is maximal for $\varphi = 0°$. The minimum at $\varphi = 29.4°$ ($R = 3.36$ Å; $X = 0.0$ Å; $Y = 0.0$ Å; $\varphi = 29.4°$) represents the global minimum of the complete dimer PES.[41] It will be called SP1 (stationary point 1) in the following. The global minimum lies about 12 kcal mol^{-1} below the fully eclipsed structure ($X = Y = 0$ Å; $\varphi = 0°$). For SP1, the binding energy of the dimer is about 28 kcal mol^{-1}. Another maximum is seen at about $\varphi \approx 60°$, which again results from unfavorable electrostatic interactions. For $\varphi \approx 90°$, the dispersion contribution to the binding is minimal. However, because the electrostatic interactions are less repulsive, this arrangement represents a local minimum. Figure 3 together with Table 1, which summarizes the computed relative energies of the lowest stationary points, underline the importance of the dispersion contribution to the total binding energy. However, its variation as a function of the geometrical arrangement of both monomers with respect to each other is rather smooth. Hence, the shape of the potential is more significantly determined by the electrostatic interactions, which are a stronger function of the geometrical parameters.

To investigate if additional minima appear for $\varphi \approx 30°$, the relative positions of the monomers with respect to each other were varied along longitudinal (X) and transversal displacements (Y) (see Figure 2). In this scan, the distance between the monomers was kept fixed at $R = 3.4$ Å. The results are depicted in Figure 4. The relative energies on the surface are color coded from blue (low energy = strong attraction of both monomers) to red (higher energy = weaker attraction of both monomers). Figure 4 shows a very shallow valley, which is about 5 Å wide along the longitudinal displacement and about 1 Å along the transversal one. The minimum of the valley at $X = Y = 0$ Å corresponds to SP1. The energy difference between this point and $X = 2$ Å and $Y = 1.0$ Å is only about 2 kcal mol^{-1}. The small increase in energy explains why already weak steric interactions due to substituents influence the arrangement of the PBI monomers within the crystal structure considerably.

Most crystal structures of substituted PBIs show arrangements in which the PBI cores are not twisted but shifted with respect to each other ($\varphi = 0°$; $X \neq Y \neq 0$ Å). Hence, X and Y were also varied for $\varphi = 0°$ to locate further stationary points on the

(39) Dennington, R., II; Keith, T.; Millam, J.; Eppinnett, K.; Hovell, W. L.; Gilliland, R. *GaussView, Version 3.07*; Semichem, Inc.: Shawnee Mission, KS, 2003.
(40) Helgaker, T.; Jørgensen, P.; Olsen, J. *Molecular Electronic Structure Theory. Energy and Wave Functions*; Wiley: Chichester, 2000.

(41) The dimer structure in which both PBI cores lie side by side, only bonded by hydrogen bridges, possesses a bonding energy of only 12 kcal mol^{-1}. This is about 10−15 kcal mol^{-1} above the global minimum SP1.

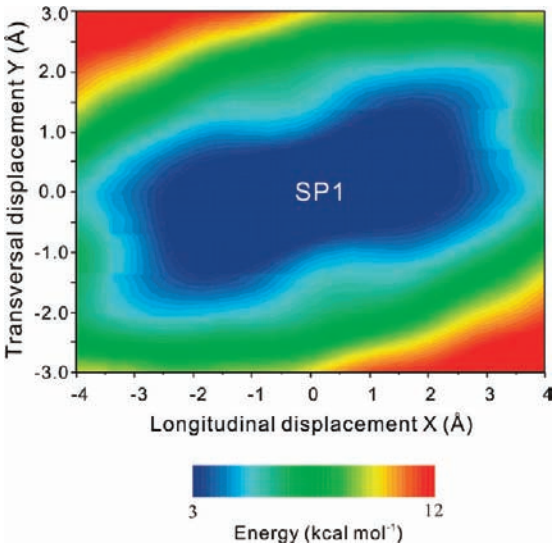

Figure 4. Potential energy surface of the dimer with $\varphi = 30°$ as a function of longitudinal (X) and transversal (Y) displacement. SP1 denotes the position of the global minimum (see text).

potential energy surface. The resulting surface is given in Figure 5. While the 3D picture of Figure 5a allows a better overall view of the shape, Figure 5b provides a contour plot. As for Figure 3, X and Y represent the displacement of the center of one monomer with respect to the center of the second monomer (Figure 2). Because of the symmetry of the dimer, the energy $E(X,Y)$ is identical to $E(-X,Y)$, $E(X,-Y)$, and $E(-X,-Y)$. The relative energies of the various stationary points and their geometrical structures are collected in Table 1. The $\varphi = 0°$ surface shows six low-lying symmetry-unique stationary points. SP2 ($R = 3.36$ Å; $X = 0.92$ Å; $Y = 1.40$ Å; $\varphi = 0°$) is the energetically lowest one. It lies 4 kcal mol^{-1} above the twisted global minimum SP1. For SP2, the monomers are shifted with respect to each other such that the electrostatic repulsion of the eclipsed structures is considerably weakened. The stationary point SP3 ($R = 3.40$ Å; $X = 1.54$ Å; $Y = 0.0$ Å; $\varphi = 0°$) represents a transition state between two SP2 arrangements. It lies about 1−2 kcal mol^{-1} higher in energy than SP2, that is, 6 kcal mol^{-1} above the global minimum SP1. The next low-lying local minimum SP4 ($R = 3.35$ Å; $X = 3.39$ Å; $Y = 1.20$ Å; $\varphi = 0°$) is only slightly higher than SP2 (<1 kcal mol^{-1}). The stationary point SP5 is found for $X \approx 3$ Å. The PES shows two shallow minima with $Y \approx 0.1$ and -0.1 Å, which are connected by a small barrier. Their barriers toward the minimum SP4 are also small. The energy variations in this region (-0.5 Å $< Y <$ 0.5 Å) are less than 1 kcal mol^{-1}. Thus, the barriers are expected to become insignificant when dynamic and temperature effects are taken into account. The whole region lies about 7 kcal mol^{-1} above the global minimum SP1, that is, only 3 kcal mol^{-1} above the minima SP2 or SP4. The stationary point SP6 ($R = 3.31$ Å; $X = 5.23$ Å; $Y = 1.43$ Å; $\varphi = 0°$) finally represents the transition state to SP7 ($R = 3.45$ Å; $X = 5.58$ Å; $Y = 0.00$ Å; $\varphi = 0°$). While SP7 lies 8 kcal mol^{-1} above the global minimum, the transition state SP6 is about 9 kcal mol^{-1} higher in energy. For SP7, the center of the second monomer lies directly above the imide nitrogen atom of the first one.

In addition to $\varphi = 0°$ and 30°, X and Y were also varied for $\varphi = 60°$ and 90°. Within the grid computations, two additional minima were found for $\varphi = 60°$, but they converged to the SP1 arrangement in the subsequent optimization without constraints. Two additional minima detected for $\varphi = 90°$ remained extra minima after the optimization without constraint (SP8, $R = 3.4$ Å, $X = 0.0$ Å, $Y = 0.0$ Å; SP9, $R = 3.4$ Å, $X = 0.0$ Å, $Y = 2.1$ Å; see Supporting Information). They are about 7 kcal mol^{-1} above the global minimum SP1.[42]

The various stationary points differ considerably in X, Y, and φ, but the distance between the monomers (R) varies only slightly ($\Delta R \approx 0.1$ Å). The distance between the monomers is mostly determined by the attractive dispersion interaction, which changes as $1/R^6$, and by the repulsive Pauli repulsion, which decreases exponentially with R. Thus, these interaction terms change rather rapidly with R but only weakly with longitudinal (X) and transversal (Y) shifts. The electrostatic interactions change more slowly as a function of R (roughly as $1/R$), but the positively and negatively charged parts of the PBI cores interact nonmonotonously for changes of X, Y, and φ. Thus, the shapes of the PESs are mainly determined by these parameters. The flatness of the computed surfaces and the various local minima indicate that the monomer units of PBI aggregates can be shifted easily with respect to each other in longitudinal and transversal direction. This is in line with the polymorphism of several PBI pigments and with findings of Zykova-Timan et al.,[15] who predicted various polymorphs for the PBI-derivative with R = CH_3 on the basis of force field computations in combination with metadynamics studies. The shallow surface also explains nicely why substituents strongly influence the crystal structures of substituted PBIs. Already, small steric effects, which may result from differences in the spatial requirements of the substituents within three-dimensional arrangements, will lead to strong variations in the crystal structures of substituted PBIs.

Nevertheless, a closer look at the computed stationary points shows that they can be correlated to the crystal structures investigated by Klebe et al.[9] This is done in Table 2, which contains the experimentally measured longitudinal and transversal shifts of the structures together with the correlation to the computed dimer PES. In this table and in the following text, the numbering of Klebe et al.[9] is used for the PBI derivatives. The different structures of polymorphic pigments are indicated by, for example, 3.1 and 3.2. Table 2 does not contain the structures 2.1 and 2.2 (R = CH_2CH_3) from the investigation of Klebe et al.[9] In structure 2.1, the PBI cores are not shifted with respect to each other but twisted ($\varphi \approx 30°$, $X = Y = 0$ Å).[9] Hence, this structure can be correlated with the twisted SP1 structure. In structure 2.2, the two PBI cores are also rotated with respect to each other, but in addition they are also slightly shifted. Considering the flatness of the computed PES for $\varphi = 30°$ as a function of X and Y (see Figure 4), this structure can also be correlated with SP1. The data set of Klebe et al.[9] contains only two examples for twisted structures. Yet they seem to be more common because several of them without[43] and with additional transversal and longitudinal shifts[44] were described. Previous studies on PBI aggregates in solution also indicate that SP1 represents a minimum, for example, for R = 3,4,5-tris-(*n*-dodecyl)phenyl in methylcyclohexane.[8b]

(42) Because these minima were not considered in the following, no zero-point vibrational corrections were determined.

(43) (a) Mizuguchi, J.; Tojo, K. *Z. Kristallogr.-New Cryst. Struct.* **2002**, *217*, 247. (b) Hino, K.; Sato, K.; Takahashi, H.; Suzuki, S.; Mizuguchi, J. *Acta Crystallogr., Sect. E* **2005**, *61*, o440. (c) Hädicke, E.; Gräser, F. *Acta Crystallogr., Sect. C* **1986**, *42*, 195.

(44) (a) Mizuguchi, J.; Hiino, K.; Sato, K.; Takahashi, H.; Suzuki, S. *Acta Crystallogr., Sect. E* **2005**, *61*, o437. (b) Tojo, K.; Mizuguchi, J. *Z. Kristallogr.-New Cryst. Struct.* **2002**, *217*, 517. (c) Zugemeier, P.; Duff, J.; Bluhm, T. L. *Cryst. Res. Technol.* **2000**, *35*, 1085.

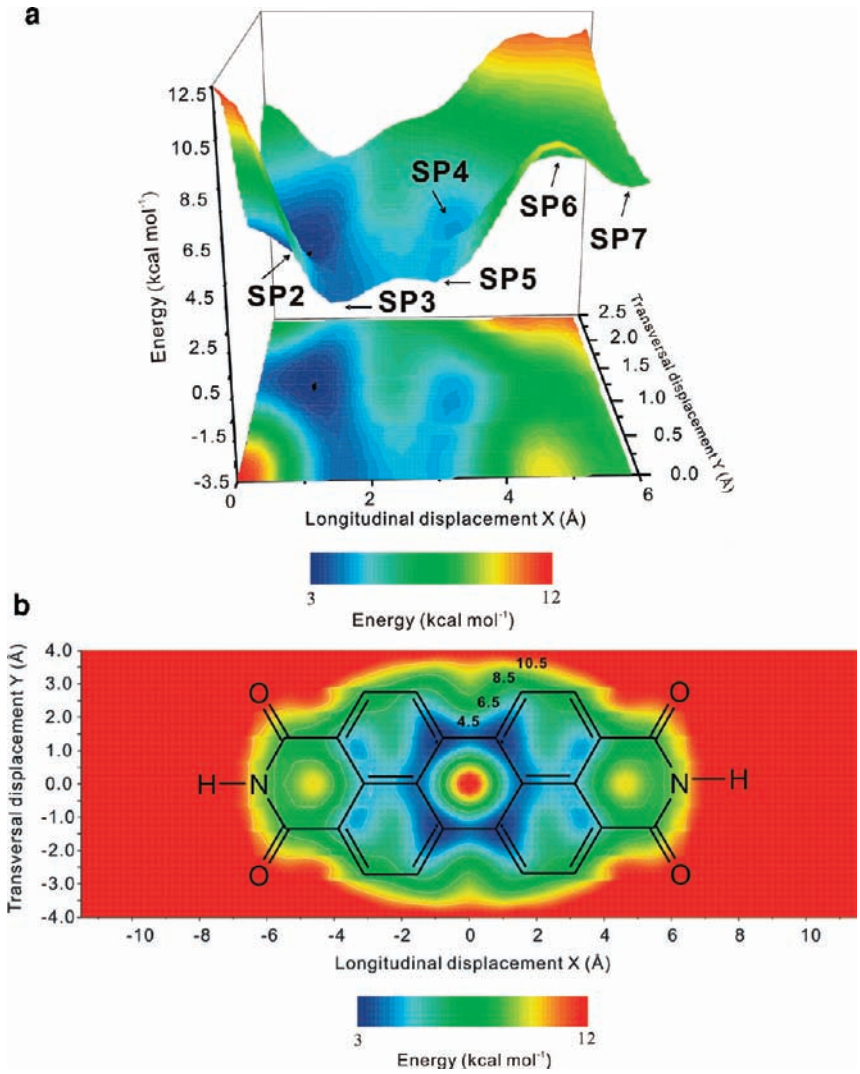

Figure 5. (a) Potential energy surface as a function of longitudinal (X) and transversal displacement (Y). The torsion angle φ is fixed at 0°. The various stationary points (SP) are denoted. (b) Potential energy surface of the PBI dimer as a function of longitudinal (X) and transversal displacement (Y). The torsion angle φ is fixed at 0°. The distance between both PBI cores is 3.4 Å. The color scale indicates the relative energies of the arrangements in which the second PBI monomer stands relative to the explicitly drawn first monomer.

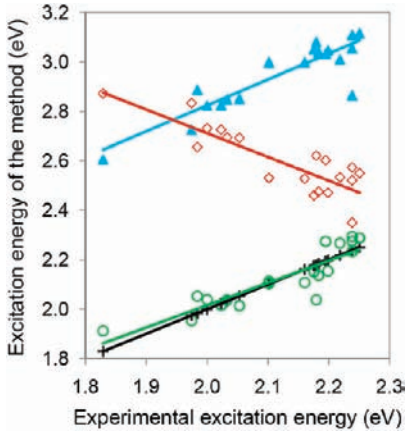

Figure 6. Correlation between predicted and measured excitation energies of the absorption maxima. Black, experimental data; green (circles), empirical fit by Klebe et al.;[9] red (diamonds), TD-B3LYP results; blue (triangles), TD-HF values. For more information, see the text.

The nuclear arrangement of the minimum SP2 can be correlated with the crystal structure found for the methyl-substituted PBI derivative (structure 1). In various crystal structures investigated by Klebe et al.,[9] the X-values range from 3.0 to 3.2 Å, while they adopt Y-values between 1.1 and 1.3 Å (structures 4, 5, 7, 9, 11.1, 12). Taking the shallowness of the computed surface into account, these arrangements can be correlated clearly with SP4 (X = 3.4 Å; Y = 1.2 Å). The structures 3.2, 8, 10.1, 10.2, 11.2, and 14 cluster around the same X-value (3.1−3.2 Å) but exhibit smaller Y-values (0.4−0.8 Å). They can be matched to the valley around SP5. Finally, structure 6 (X = 5.5 Å, Y = 1.0 Å) can be correlated with the region around the stationary points SP6 (X = 5.2 Å, Y = 1.4 Å) and SP7 (X = 5.6 Å, Y = 0.0 Å). In our computations, minimum SP7 is found for Y = 0 Å, but the energy difference to the saddle point SP6 is only around 1 kcal mol^{-1}. Finally, the relative orientation of neighboring PBI cores found for structure 13 (X = 2.7 Å, Y = 0.4 Å) is between SP3 and SP5. Although there is no stationary point in this region, it is still quite low in energy. These correlations indicate that, despite the flatness of the dimer surface, the interactions between the PBI cores still play an important role in the formation of PBI crystals. Structures 3.1 and 15−18.2 show that nevertheless cases exist for which the interactions between the PBI cores

Table 2. Measured Longitudinal (*X*) and Transversal (*Y*) Shifts of the Crystal Structures Investigated by Klebe et al.[9] [a]

struct.[b]	substituent	*X*	*Y*	*R*	corr.[c]
1	$-CH_3$	0.94	1.60	3.400	SP2
3.1	$-CH_2-CH_2-CH_3$	2.05	2.48	3.411	−
3.2	$-CH_2-CH_2-CH_3$	3.11	0.79	3.408	SP5
4	$-(CH_2)_3-CH_3$	3.10	1.11	3.402	SP4
5	$-(CH_2)_4-CH_3$	3.11	1.31	3.343	SP4
6	$-CH_2-CH(CH_3)-CH_2-CH_3$	5.45	0.98	3.422	SP6−SP7
7	$-CH_2-CH_2-O-CH_2-CH_3$	3.23	1.28	3.355	SP4
8	$-CH_2-CH_2-CH_2-O-CH_3$	3.15	0.68	3.455	SP5
9	$-CH_2-CH_2-CH_2-O-CH_2-CH_3$	3.06	1.26	3.402	SP4
10.1	$-(CH_2)_4-OH$	3.22	0.76	3.355	SP5
10.2	$-(CH_2)_4-OH$	3.06	0.70	3.510	SP5
11.1	$-(CH_2)_6-OH$	3.19	1.10	3.395	SP4
11.2	$-(CH_2)_6-OH$	3.13	0.85	3.415	SP5
12	$-CH_2-C_6H_5$	3.08	1.10	3.425	SP4
13	$-CH_2-p-C_6H_4-OCH_3$	2.67	0.36	3.459	SP3−SP5
14	$-CH_2-CH_2-C_6H_5$	3.20	0.39	3.476	SP5
15	$-CH_2-CHCH_3-C_6H_5$	1.23	3.40	3.426	−
16.1	$-p-C_6H_4-O-CH_2-CH_3$	1.56	3.09	3.550	−
16.2	$-p-C_6H_4-O-CH_2-CH_3$	0.55	3.50	3.470	−
17	$-p-C_6H_4-N=N-C_6H_5$	0.81	3.96	3.480	−
18.1	$-C_6H_4-(CH_3)_2$	2.97	2.69	6.653	−
18.2	$-C_6H_4-(CH_3)_2$	3.10	6.57	2.749	−

[a] Distances are given in angstroms. [b] The crystal structures are designated by the numbering of the PBI derivatives according to the work of Klebe et al.[9] Polymorphic structures are named as, for example, 3.1 and 3.2. [c] Stationary point to which the crystal structure can be correlated (see text).

are less important for the stability of the observed crystal structure. For structures 15−18.2, the interactions between both cores are already quite weak, because the overlap between the PBI cores decreases considerably. In such cases, steric effects arising from the substituents become dominant, although the interaction between the PBI cores will still contribute to the overall binding. The dominance of these other effects for structures 15−18.2 is in line with the rather bulky substituents in the corresponding compounds.

Computed Vertical Excitation Energies. In dilute solution or in molecular dispersion, as for example in polystyrene, where short-range interaction between PBI molecules can be excluded, all substituted PBI pigments exhibit an orange color. They show almost identical absorption spectra, which are dominated by the very strong transition into the 1^1B_{1u} state of the monomer. The absorption maxima of PBI crystals, however, span a wide range of more than 170 nm, leading to very different colors, such as red, maroon, and black. To study the reasons for the large color range in more detail, the vertical excitation energies of the crystal structures discussed by Klebe et al.[9] were calculated. The calculations were actually done for unsubstituted dimers, but higher-order effects due to the crystal surrounding were approximated (vide infra). The orientations of the monomer units with respect to each other were taken from the crystal structure data. As in the preceding ground-state investigation, the intramolecular PBI structures were the ones obtained for the monomer at the BLYP-D/TZV(P) level. As a first step, the excited states of these dimer structures and of the monomer were calculated with the TD-HF/TZV(P) and the TD-B3LYP/TZV(P) methods. The TD-HF method provided only two low-lying excited states, which turned out to be dominated by the plus and minus linear combinations of the locally excited monomers. Their energy separation is the so-called Davydov splitting. The dominating neutral configurations in such electronic states are going to be designated as locally excited configurations in the following. In contrast, the TD-B3LYP method provides various low-lying excited states, which, in line with previous investigations for similar systems,[26,27] result from admixture of low-lying charge-transfer configurations to the locally excited configurations.

It is well established that the Davydov splitting results from the electronic coupling of the excited states of two molecules.[45−47] This coupling is dominated by a dipole−dipole term of the oscillating transition dipoles of the excitation process. However, due to the close packing for adjacent chromophores in the crystal structures, additional so-called Dexter interactions[48] become significant. Both interactions are properly represented by the supermolecule approaches for the dimer applied in the present work. However, dimer calculations only account for parts of the actual interactions within crystals, which are most commonly arranged in stacks with parallel orientation of the flat PBI cores. In particular, the identical interaction with the other nearest neighbor in the π stack (on the opposite site) is missing. Yet even the interactions to the next but one neighbor cannot be neglected as the leading dipole−dipole interaction decays relatively slowly as $1/R^3$, where R is the distance between the monomer centers. The importance of such interactions was also underlined by a recent paper of Gierschner et al.[49] The missing interactions could in principle also be calculated with the supermolecule approach. However, the relatively slow ($1/R^3$) convergence of the dipole−dipole interaction and additional difficulties resulting from the dynamic polarization of the molecules between the donor and acceptor PBIs[50−52] would make such an approach too demanding. For that reason, we approximate the missing interactions by assuming that the interactions of the PBI molecules along the π stack decay according to the dipole−dipole rule. Interactions to molecules not belonging to the π stack are neglected. Using this assumption, the absorption band maximum in the solid is calculated to be at the energy

$$\Delta E_s \approx 2\cdot\left(1+\frac{1}{2^3}+\frac{1}{3^3}+\frac{1}{4^3}+\frac{1}{5^3}+\ldots\right)(\Delta E_d-\Delta E_m)+\Delta E_m = 2\cdot\zeta(3)\cdot(\Delta E_d-\Delta E_m)+\Delta E_m \quad (1)$$

where $\zeta(3) \approx 1.202056$ is Apéry's constant.[53] ΔE_d and ΔE_m are the excitation energies calculated for the dimer and monomer, respectively. As a consequence, in this approximation, the Davydov splitting of the PBI chromophores in a crystal is larger by a factor of about 2.4 than in the dimer. Please note that additional polarization and screening effects arising due to the crystal environment are not taken into account. Such effects are expected to lower both kinds of states, and furthermore they may lower the CT states with respect to the neutral states.

(45) Kasha, M.; Rawls, H. R.; Ashraf El-Bayoumi, M. *Pure Appl. Chem.* **1965**, *11*, 371–380.
(46) Scholes, G. D. *Annu. Rev. Phys. Chem.* **2003**, *54*, 57–87.
(47) May, V.; Kühn, O. *Charge and Energy Transfer Dynamics in Molecular Systems*, 2nd ed.; Wiley−VCH: Weinheim, 2004.
(48) Dexter, D. L. *J. Chem. Phys.* **1953**, *21*, 836–840.
(49) Gierschner, J.; Huang, Y. S.; van Averbeke, B.; Cornil, J.; Friend, R. H.; Beljonne, D. *J. Chem. Phys.* **2009**, *130*, 044105.
(50) Fückel, B.; Köhn, A.; Harding, M. E.; Diezemann, G.; Hinze, G. *J. Chem. Phys.* **2008**, *128*, 074505-1–074505-13.
(51) (a) Scholes, G. D.; Curutchet, C.; Mennucci, B.; Cammi, R.; Tomasi, J. *J. Phys. Chem. B* **2007**, *111*, 6979–6982. (b) Scholes, G. D. *Annu. Rev. Phys. Chem.* **2003**, *54*, 57–84.
(52) Scholz, R.; Kobitski, A. Y.; Zahn, D. R. T.; Schreiber, M. *Phys. Rev. B* **2005**, *72*, 245208.
(53) (a) Havil, J. *Gamma: Exploring Euler's Constant*; Princeton University Press: Princeton, NJ, 2003. (b) Steuding, J. *Diophantine Analysis*; CRC-Press/Chapman & Hall: Boca Raton, FL, 2005.

Table 3. Comparison between the Measured and Computed Energy Positions of the Absorption Maxima

		[a]experimental		TD-HF	
struct.[a]	substituent	η_{max} (nm)	[b]EE (eV)	[c]ΔE_{shift} (eV)	[d]error (eV)
1	$-CH_3$	569	2.18	2.25	−0.07
3.1	$-CH_2-CH_2-CH_3$	559	2.22	2.18	0.04
3.2	$-CH_2-CH_2-CH_3$	610	2.03	2.02	0.01
4	$-(CH_2)_3-CH_3$	574	2.16	2.17	−0.01
5	$-(CH_2)_4-CH_3$	570	2.18	2.22	−0.05
6	$-CH_2-CH(CH_3)-CH_2-CH_3$	554	2.24	2.04	0.20
7	$-CH_2-CH_2-O-CH_2-CH_3$	564	2.20	2.22	−0.02
8	$-CH_2-CH_2-CH_2-O-CH_3$	613	2.02	1.99	0.03
9	$-CH_2-CH_2-CH_2-O-CH_2-CH_3$	568	2.18	2.21	−0.03
10.1	$-(CH_2)_4-OH$	620	2.00	1.99	0.01
10.2	$-(CH_2)_4-OH$	604	2.05	2.02	0.03
11.1	$-(CH_2)_6-OH$	590	2.10	2.17	−0.07
11.2	$-(CH_2)_6-OH$	625	1.98	2.06	−0.07
12	$-CH_2-C_6H_5$	590	2.10	2.17	−0.07
13	$-CH_2-p\text{-}C_6H_4-OCH_3$	678	1.83	1.78	0.05
14	$-CH_2-CH_2-C_6H_5$	628	1.97	1.90	0.08
15	$-CH_2-CHCH_3-C_6H_5$	551	2.25	2.29	−0.04
16.1	$-p\text{-}C_6H_4-O-CH_2-CH_3$	554	2.24	2.28	−0.04
16.2	$-p\text{-}C_6H_4-O-CH_2-CH_3$	554	2.24	2.22	0.01
17	$-p\text{-}C_6H_4-N{=}N-C_6H_5$	565	2.19	2.20	−0.01

[a] Numbering is taken from Klebe et al.[9] [b] Excitation energy in eV. [c] $\Delta E_{shift} = \Delta E_s - 0.84$ eV (see eq 1 and text). [d] Difference between shifted TD-HF value and experiment.

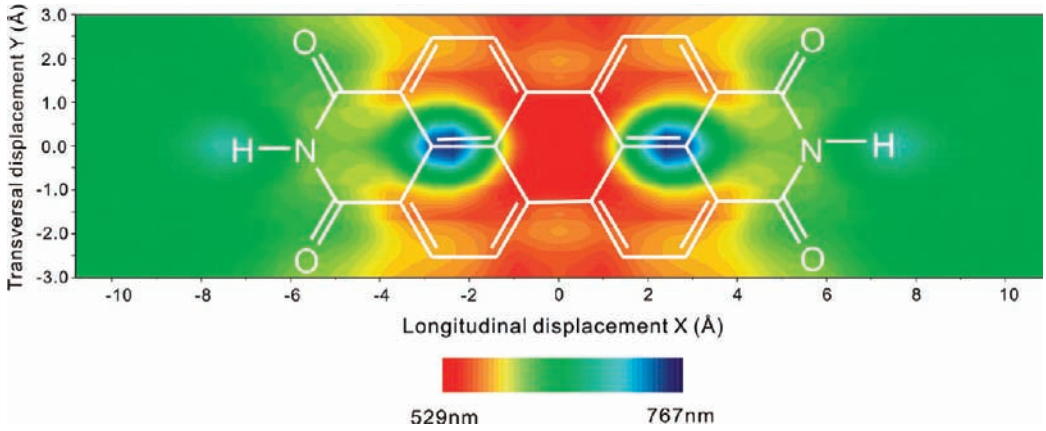

Figure 7. Computed vertical excitation energies from the electronic ground state to the state with the largest transition dipole moment (TDM) as a function of the longitudinal (X) and the transversal shift (Y) of the dimer. For more information, see the text.

To compute the maxima of the absorption of the crystal, eq 1 was applied to the excited state of the dimer with the most intense transition. In the TD-HF approach for which only two low-lying states have been obtained, this is clearly the state dominated by the plus linear combination of the locally excited configurations. In all cases investigated, the plus linear combination represents the upper state. For the TD-B3LYP level of theory, however, the choice is less clear because several electronic states with varying transition moments have been found. Typically the energetically lowest one is a charge-transfer state with a quite low transition probability. Several states with higher intensities then follow. We always applied eq 1 to the state with the highest transition dipole moment. This turned out to be the one that is dominated by the plus combination of the locally excited configurations. The resulting excitation energies for the crystal structures discussed by Klebe et al.[9] are depicted in Figure 6. For comparison, it also gives the experimental results, the fitted excitation maxima of Klebe et al.,[9] and theoretical data obtained in the same manner as the TD-HF data but with TD-B3LYP excitation energies.

Figure 6 shows that TD-HF predicts the trend of the Davydov splitting very well albeit with a significant blue shift that is typically observed for this method. On average, the calculated TD-HF excitation energies are too high by 0.84 eV. Such a shift is expected for the TD-HF method, which generally tends to overestimate excitation energies. Table 3 shows the shifted excitation energies ($\Delta E_{shift} = \Delta E_s - 0.84$ eV) and the measured data with the corresponding substitution pattern. As Klebe et al.[9] did, we excluded the twisted structures 2. Structures 18.1 and 18.2 were also excluded as the monomers are so far away from each other that the present dimer approach is no longer reasonable. The shifted excitation energies (ΔE_{shift}) predict the measured energy positions of the absorption maxima with deviations of less than 0.1 eV. The exception, structure 6, may result from the substantial longitudinal shift of next-neighbor PBI moieties in this pigment such that dimer interactions become less dominant.

In contrast, TD-B3LYP predicts a wrong trend. The red-shifted PBI structures are predicted to be blue-shifted and vice versa. The failure of the TD-B3LYP approach is astonishing at the first glance. The maxima of the absorption spectra are assigned with excitation into low-lying excited neutral states, which possess considerably higher transition dipole moments for the transition from the ground states than the CT states.

Neutral states, however, are in most cases nicely described by TD-DFT. An explanation for the failure of TD-DFT could be that it underestimates the energy position of CT states. As neutral and CT states of the same symmetry interact with each other, an underestimation of the energy position of the CT state can very well cause an erratic behavior of the neutral state energy. Test calculations indicate that TD-BHLYP, which yields good results for some organic excimers,[54] predicts the right trend, but the slope is much too steep.

As shown above, our approach (TD-HF excitation energies for the respective dimer scaled by eq 1 and shifted by −0.84 eV) is able to reproduce the excitation energies of PBI crystal structures rather reliably. To predict the color of yet unknown crystal structures, we employed this model to compute absorption maxima of crystal structures in which the PBI cores are longitudinally (-11 Å $< X <$ 11 Å) and transversally (-3 Å $< Y <$ 3 Å) shifted relative to each other.[55] The distance between two monomers was again fixed at $R = 3.4$ Å. Figure 7 shows the corresponding color-coded vertical dimer excitation energies to the state with the highest transition dipole moment.

4. Summary and Conclusions

A theoretical protocol has been presented here, which allows accurate predictions of the packing and optical properties of perylene tetracarboxylic bisimide (PBI) pigments and offers insight into the effects that determine these properties. In a first step, the ground-state energy surface of an unsubstituted PBI dimer has been computed for different torsion angles φ as a function of longitudinal (X) and transversal (Y) shifts. The resulting potential-energy surfaces (PESs) are very flat, which nicely explains why already small variations in the substitution pattern can lead to strong alterations in the crystal structures. A comparison between the minima of the PESs and 22 different crystal structures shows, however, that most structures can still be correlated with minima of the unsubstituted dimer. This indicates that the interactions between the PBI cores have a major influence on the three-dimensional organization of the PBI monomers in the crystal structures of differently substituted PBI derivatives. While dispersion effects are important for the overall binding, the shape of the PES is determined by electrostatic interactions (e.g., quadrupole moments).

In a second step, vertical excitation energies to low-lying electronically excited states have been computed for 20 different crystal structures. The computations use excitation energies of dimers and approximate higher order effects, which result from the crystal packing. The excitation energies of the transitions with the highest transition moments have been compared to the measured photon energies at the absorption maxima of the 22 different pigment structures. The trend computed with TD-HF agrees almost perfectly with experimental data, while TD-B3LYP predicts the wrong trend. In both computations, the transitions to the excited neutral states were taken into account to describe the variations in the energy position of the absorption maxima as these states possess considerably higher transition dipole moments.

Because neutral states should be described nicely by both TD-HF and TD-B3LYP, the failure of TD-B3LYP is astonishing. The difference between TD-HF and TD-B3LYP is likely due to the well-known trend of these methods to describe the energies of neutral and CT configurations. TD-HF predicts the CT configurations at considerably higher energies than those of neutral configurations. As a consequence, in this picture CT states are well separated from neutral ones and have only a minor influence on the optical properties of PBI aggregates. TD-B3LYP predicts CT configurations at considerably lower energy so that a reverse energy order and considerably smaller energy separations result. Hence, in this approach, the admixture of CT and neutral configurations is considerably stronger and shifts the energy position of the neutral states in the opposite direction. Because of the underestimation of energy position of CT states in the TD-DFT picture, this approach predicts them to be very important for the optical properties. While the interactions described by TD-DFT seem to be questionable, the present success of TD-HF does not definitely rule out an influence of CT states on the visible light absorption properties of PBI pigments. It might be that in reality their influence is considerably stronger than predicted by TD-HF but constant for all investigated crystal structures.

Acknowledgment. Financial support by the DFG (Deutsche Forschungsgemeinschaft) (GRK1221) and the Volkswagen Stiftung (B.E. and R.F.F.) is gratefully acknowledged. Dedicated to W. A. Schenk on the occasion of his 65th birthday.

Supporting Information Available: Cartesian coordinates, quadrupole moments, and complete ref 38. This material is available free of charge via the Internet at http://pubs.acs.org.

JA902512E

(54) Hünerbein, R.; Grimme, S. *Chem. Phys.* **2008**, *343*, 362–371.
(55) The computations were performed for 0 Å $< X <$ 6 Å and 0 Å $< Y <$ 3 Å. The remaining parts result from the D_2 symmetry of the system.